agriculture

Article

Using RGB Imaging, Optimized Three-Band Spectral Indices, and a Decision Tree Model to Assess Orange Fruit Quality

Hoda Galal [1], Salah Elsayed [2,*], Osama Elsherbiny [3], Aida Allam [1] and Mohamed Farouk [4]

[1] Evaluation of Natural Resources Department, Environmental Studies and Research Institute, University of Sadat City, Menoufia 32897, Egypt
[2] Agricultural Engineering, Evaluation of Natural Resources Department, Environmental Studies and Research Institute, University of Sadat City, Menoufia 32897, Egypt
[3] Agricultural Engineering Department, Faculty of Agriculture, Mansoura University, Mansoura 35516, Egypt
[4] Agricultural Engineering, Surveying of Natural Resources in Environmental Systems Department, Environmental Studies and Research Institute, University of Sadat City, Menoufia 32897, Egypt
* Correspondence: salah.emam@esri.usc.edu.eg

Abstract: Point samples and laboratory testing have historically been used to evaluate fruit quality criteria. Although this method is precise, it is slow, expensive, and destructive, making it unsuitable for large-scale monitoring of these parameters. The main objective of this research was to develop a non-invasive protocol by combining color RGB indices (CIs) and previously published and newly developed three-band spectral reflectance indices (SRIs) with a decision tree (DT) model to evaluate the fruit quality parameters of navel orange. These parameters were brightness (L*), red–green (a*), blue–yellow (b*), chlorophyll meter (Chlm), total soluble solids (TSS), and TSS/acid ratio. The characteristics of fruit quality of navel orange samples were measured at various stages of ripening. The outcomes demonstrated that at various levels of ripening, the fruit quality parameters, RGB imaging indices, and published and newly developed three-band SRIs differed. The newly developed three-band SRIs based on the wavelengths of blue, green, red, red-edge, and NIR are most effective for estimating the six measured parameters in this study. For example, $NDI_{574,592,724}$, $NDI_{572,584,724}$, and $NDI_{574,722,590}$ had the largest R^2 value (0.90) with L*, whereas $NDI_{526,664,700}$ and $NDI_{524,700,664}$ exhibited the highest R^2 value (0.97) with a*. Moreover, integrating CIs and SRIs with the DT model has provided a potentially useful tool for the accurate measurement of the six studied parameters. For instance, the DT-SRIs-CIs-30 model performed better in terms of measuring a* using 30 various indices. The R^2 value was 0.98 and RMSE = 1.121 in the cross-validation, while R^2 value was 0.964 and RMSE = 2.604 in the test set. Otherwise, based on the fusion of five various indices, the DT-SRIs-CIs-5 model was the most precise for recognizing b* (R^2 = 0.957 and 0.929, with RMSE = 1.713 and 3.309 for cross-validation and test set, respectively). Overall, this work proves that integrating the different characteristics of proximal reflectance sensing systems such as color RGB indices and SRIs via the DT model may be considered a reliable instrument for evaluating the quality of different fruits.

Keywords: decision tree model; proximal reflectance sensing RGB; indices; three-band; orange

check for updates

Citation: Galal, H.; Elsayed, S.; Elsherbiny, O.; Allam, A.; Farouk, M. Using RGB Imaging, Optimized Three-Band Spectral Indices, and a Decision Tree Model to Assess Orange Fruit Quality. *Agriculture* **2022**, *12*, 1558. https://doi.org/10.3390/agriculture12101558

Academic Editor: Hongbin Pu

Received: 6 August 2022
Accepted: 21 September 2022
Published: 27 September 2022

Publisher's Note: MDPI stays neutral with regard to jurisdictional claims in published maps and institutional affiliations.

Copyright: © 2022 by the authors. Licensee MDPI, Basel, Switzerland. This article is an open access article distributed under the terms and conditions of the Creative Commons Attribution (CC BY) license (https://creativecommons.org/licenses/by/4.0/).

1. Introduction

Citrus is a common and widely grown fruit crop in more than 140 nations worldwide [1]. In Egypt, the orange industry and exporting are significant contributors to the national economy. Navel oranges are the most widely grown citrus group and account for around 47.1% of citrus growing area and 51.8% of total production [2]. The production and exporting of oranges have steadily increased over the previous three decades, with Egypt becoming the world's first orange exporter in 2020. Egyptian navel oranges are mostly exported to nations in the Arab Gulf and the European Union [1]. The required fruit quality range varies by market and includes fruit size, color, and some internal chemical characteristics such as total soluble solids (TSS), juice acidity, and TSS/acidity ratio [3–5].

The fruit undergoes dramatic physiological and chemical changes during growth and maturation, resulting in significant variations in fruit size, texture, color, and flavor. Furthermore, citrus fruits, like non-climacteric fruits, do not ripen after being picked. As a result, fruits must achieve the appropriate ripening stage before harvesting. Many criteria can be considered when determining the ideal time to harvest, including the number of days from bloom to harvest; the formation of the abscission zone; and changes in color, taste, aroma, firmness, and internal chemical components [6–8]. All of the above traits depend on either personal judgment or destructive and time-consuming procedures. In earlier times, humans relied on their ability to distinguish between ripe and unripe crops through their vision. However, due to distraction, attention, and other things that occurred while working, this system had a significant mistake rate [9]. In addition, laboratory tests are unable to track quick changes in biochemical characteristics as a result of environmental changes [10]. Laboratory testing and point samples were used to estimate the fruit quality parameters. This technique is effective for monitoring these indicators, but it is slow, expensive, hazardous, and geographically constrained. Additionally, it cannot be used to provide decision-makers with a comprehensive evaluation of crucial indicators linked to fruit quality on a large field scale and for a huge number of fruit samples [11–13].

Spectroscopy is a cutting-edge scientific technique that has recently attracted a lot of attention. It allows access to information about the chemical components and physical qualities of fruits by obtaining optical information, while imaging methods enable obtaining pictures of fruits and gaining their visual relationships [14–16]. Visible and near-infrared (Vis/NIR) radiation has wavelengths of between 300 and 2500 nm, and it is a component of the electromagnetic spectrum that may be detected by passive or active reflectance sensors. The Vis/NIR spectrum is frequently used in research because it can reliably distinguish the signals of almost all significant organic structural and functional groups with a rather stable spectrogram [15,17]. Several research studies [1–6] used proximate passive reflectance sensing and spectroscopic methods to assess the biochemical properties of distinct fruit species. For example, Elsayed et al. [11] assessed TSS, acidity, chlorophyll, and carotene using passive reflectance sensing and digital image analysis, while Hashim et al. [18] applied multispectral imaging to assess chilling injury in mangoes. Galal et al. [13] used two-band spectral reflectance indices (SRIs) of passive reflectance to assess changes in chlorophyll, firmness, respiration rate, and TSS throughout banana ripening. In addition, spectroscopy technology and remote sensing were successfully employed to measure sugar content and fruit firmness in apples [19–21] and soluble solids and total phenolic content in strawberries [22].

Digital cameras employ their own visual-based color coding, which offers dependability, high performance, and repeatable operation [23,24]. This leads to an increase in productivity and a decrease in the need for skilled labor. In digital cameras, three components of the color image are used to assess the provided fruit and vegetable image [25]. Red, green, and blue (RGB) components of a whole image can be represented by decoding a color camera output into three images. For agricultural products such as fruits, color is regarded as an essential physical characteristic [26]. The loss of green color to yellow in many orange crops is a clear indicator that the fruit is ripening. The development of the ideal skin color is often determined by the orange quality. So, the use of digital cameras with color images has been demonstrated to be a promising source for predicting numerous fruit quality characteristics. During orange ripening stages, there were decreases in the values of fruit characteristics such as hardness, starch, pulp content, and pulp:peel ratio and increases in TSS, sugar:acid ratio, pH, and carotenoid concentration [12,27]. In agriculture, RGB-based image analysis has been used to identify the carotenoids and chlorophyll in orange fruits [28] and the chlorophyll, total carbohydrates, soluble solids content, carotenoids, pH, and titratable acidity of mango fruits [11,29]. For instance, the R/G band demonstrated a sensitive band ratio to various orange characteristics, such as chlorophyll and carotenoids, as averages of RGB and the Visible Atmospheric Resistant Index (VARI) [28]. In addition, Choi et al. [30] used an outdoor machine vision system with red, green, and blue (RGB);

near-infrared (NIR); and depth sensors to count the number of immature citruses in tree canopies. In addition, Gomes-Junior et al. [31] found that the RGB color scheme may be used to create a precise categorization of fruit ripening in order to determine the ideal time to harvest for seeds with the highest physiological and storage potential. The scientific hypothesis proposed in this study analyses whether variations in orange fruit quality may be represented by changes in spectral reflectance and RGB image analysis based on the shift in skin color from dark green to yellow.

Feature selection strategies, such as the model-based feature selection method, pick a subset of characteristics with high discriminative and predictive power [32]. This strategy can enhance model performance by removing superfluous features and preventing overfitting. It also has the added benefit of retaining the original feature representation, which provides improved interpretability [33]. Feature selection algorithms are now required for prediction and modeling [34]. Many studies have looked into the use of various techniques to minimize data dimensionality. The weighted regression coefficient of each variable in the partial least squares (PLS) model illustrates the significance of the wavelength in the model for partial least square regression (PLSR) [35]. All variables are ordered according to their importance in the random forest (RF) and decision tree (DT) [36]. Glorfeld [37] developed a back-propagation neural network index that can be used to identify the most essential variables. Furthermore, hyperparameter selection has a significant impact on the performance of any machine learning model, which has multiple advantages: it can improve the performance of ML algorithms [38] and the repeatability and fairness of scientific investigations [39]. Because it has direct control over the behavior of training algorithms, it could play a significant role in refining the prediction model [40]. As a result, we may assume that hyperparameter adjustment has a considerable impact on the prediction effectiveness of quality parameters for orange fruits.

Based on our knowledge, no prior research has implemented a composite approach of decision tree models with RGB indices and SRIs for estimating fruit quality parameters. In addition, it is still necessary to develop further optimized SRIs in order to ensure the performance of SRIs as a quick and easy method to precisely estimate fruit quality parameters because spectral reflectance indices (SRIs) frequently exhibit inconsistent results in estimating the fruit quality of crops under various environmental and spatial conditions. Additionally, there is a critical need to identify the best algorithm formulations for calculating various fruit quality characteristics in order to increase the effectiveness of remotely sensed data for fruit quality assessment. In general, past research has concentrated on the use of two-band SRIs, with just a few studies using three-band SRIs to measure fruit quality parameters. The advantage of this study is that the optimum three-band SRIs were selected by building 3D correlogram maps, which provides a high ability to optimally pick the best SRIs to assess the fruit quality parameters. Consequently, the specific objectives of this work were to (i) estimate the changes in the values of the different physical parameters (brightness (L*), red–green (a*), blue–yellow (b*), and chlorophyll meter (Chlm)) as well as chemical parameters (total soluble solids (TSS), and TSS/acid ratio) of navel orange samples at different ripening degrees; (ii) extract the optimized newly developed three-band SRIs for L*, a*, b*, Chlm, TSS, and TSS/acid ratio using the 3D dimensional slice map; (iii) assess the accuracy of published and developed three-band SRIs in quantifying the six fruit quality parameters at different ripening degrees; and (iv) measure the decision tree model's accuracy in characterizing the six orange fruit parameters based on color RGB indices, SRIs, and their combinations at different ripening degrees.

2. Materials and Methods

2.1. Plant Material

Navel orange fruits were collected from a private orchard located on the Cairo–Alexandria Desert Road. Fully developed fruits in different ripening stages were chosen from October to December in 2020 and 2021. Fruits were classified into three categories based on the color of their peel. A total of 120 fruit samples were collected, where about

40 replicates each of the mature (mainly green), semi-ripening (green/yellow), and ripening (primarily yellow peel) stages shown in Figure 1 were utilized for laboratory analysis. All collected fruit samples were free from diseases, insects, or mechanical damage. Fruit samples were sent immediately to the Pomology Lab at the Environmental Studies and Research Institute, University of Sadat City, to determine the following physical and chemical characteristics.

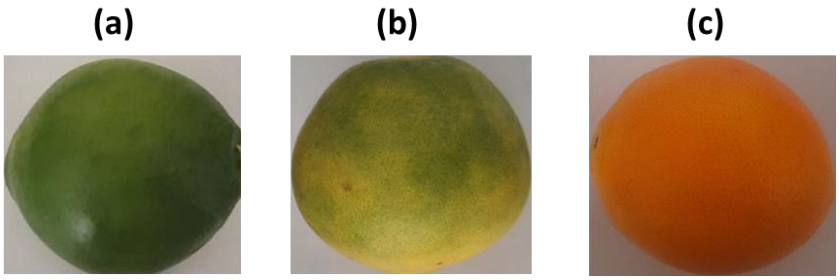


Figure 1. Fruits were classified into three categories: (**a**) mature, (**b**) semi-ripening, and (**c**) ripening.

2.2. Physical Characteristics

2.2.1. Chlorophyll Content in the Peel

The relative chlorophyll content was determined using a SPAD-502 portable chlorophyll meter (Konica-Minolta, Osaka, Japan).

2.2.2. Peel Color

A precise colorimeter (Sucolor SC-10, Shenzhen, China) was used to measure changes in peel color. The mean of three randomly chosen places of each fruit was obtained by providing the color space parameters L*, a*, and b*. According to Mc Guire [41], the L* parameter represents brightness (ranging from 0 for black to 100 for white), a* stands for negative green and positive red, and b* stands for negative blue and positive yellow.

2.3. Chemical Characteristics

2.3.1. Total Soluble Solids (TSS)

To quantify the chemical components in the fresh juice, each fruit was squeezed individually. TSS was determined using a handheld refractometer (Milwaukee, model MA871, Brookfield, WI, USA).

2.3.2. Total Soluble Solids/Titratable Acidity Ratio (TSS/Acid)

Titratable acidity was determined as grams of citric acid in 100 mL of fresh juice by titration with (0.1 N) NaOH for each fruit, in accordance with AOAC [42]. The ratio of total soluble solids to titratable acidity (TSS/acid) was then calculated.

2.4. Digital RGB Imaging

The orange fruit samples were imaged using a 14-megapixel digital camera (Kodak D5100 reflex; Tokyo, Japan) with a resolution of 2454 × 2056 pixels and 8-bit RGB images after they had been collected at various stages of ripening. At a distance of 0.5 m, the camera was manually held and pointed vertically downward at the fruit samples. The measurements were carried out under cloudy conditions to guarantee high image resolution. The flash of the camera was always kept off during measurements. The digital images were saved in the jpeg format and then analyzed using the Python software (Version 3.7.3 creator of the project programming, Osama, Mansoura, Egypt, 2022) in Supplementary Material S1. Because the images sometimes contained non-fruit features such as the background and some leaves sticking to the fruit, the images need to be segmented and extracted to eliminate interference by non-fruit features during feature extraction. The images were split and extracted in order to remove non-fruit features' interference during feature extraction because the images occasionally contained non-fruit features. To extract just the color

components from the RGB images, they were transformed into the hue, saturation, and intensity color space. Fruit pixels were then distinguished from background pixels using predetermined thresholds. The background pixels were then adjusted to 0 and the plant pixels to 1 to create a binary picture of the fruit samples [43,44]. The threshold technique is an image segmentation process that converts an image to grayscale [44] and produces a binary image [44] with two possible pixel values, namely the intensity value of the image that is greater than or equal to the threshold value of 1 (white or foreground) and less than the threshold value or value 0 (black or background) that can be removed. The binary image's pixels were 1 bit in size. Because RGB imaging is composed of three bands, the color of each pixel is divided into three values [45]. As shown in Table 1, several RGB imaging indices were examined in this study. Using the following formulae, the RGB color space percentage values were retrieved as sample features.

$$R = \frac{1}{S\ num} \sum_{i=1}^{S_{num}} R_i \quad (1)$$

$$G = \frac{1}{S\ num} \sum_{i=1}^{S_{num}} G_i \quad (2)$$

$$B = \frac{1}{S\ num} \sum_{i=1}^{S_{num}} B_i \quad (3)$$

where R, G, and B are the mean values of the red, green, and blue bands, respectively, and Ri, Gi, and Bi are the pixel values for the red, green, and blue bands, respectively, in the digital picture; I and S_{num} are the initial pixel and maximum number of pixels, respectively.

Table 1. Description of different RGB imagery indices tested in this study.

RGB Indices	Formula	References
Red pixel percentage (R %)	R/(R + G + B)	[45]
Green pixel percentage (G %)	G/(R + G + B)	[45]
Blue pixel percentage (B %)	B/(R + G + B)	[45]
Green blue ratio index (GBRI)	G/B	[46]
Woebbecke index (WI)	(G − B)/(R − G)	[47]
Excess green vegetation index (ExG)	2 × G − R − B	[48]
Excess blue vegetation index (ExB)	1.4 × bn − gn	[49]
Excess green minus excess red index (ExGR)	ExG − ExR	[50]
Vegetative index (VEG)	G/(Ra × B(1 − a)), a = 0.667	[51]
Combination (COM)	0.25 × ExG + 0.3 × ExGR + 0.33 × CIVE + 0.12 × VEG	[52]

2.5. Measuring Spectral Reflectance and Selection of SRIs of Orange Fruits

Following the collection of different orange fruit samples at various stages of ripening, the spectral information for each sample was retrieved using a passive reflectance sensor (tec5, Oberursel, Germany) with a spectral range of 302 to 1148 nm. The spectral bandwidth was 2 nm, and the field of view was 12°. The spectrometer optic was placed vertically around 25 cm at a nadir position over the fruit surface of the samples. Five different scans were performed on each orange fruit sample. Fruit samples' spectral measurements based on sunlight were taken during a brief period of time at 12 a.m. on a sunny day in order to prevent changes in light exposure. A calibration factor obtained from a reference gray standard was used to correct the reflectance data of orange samples. To achieve complete reflectance by the orange fruit and to avoid spectral reflection from the background, a black sheet was put beneath each fruit.

Twenty-four SRIs, including 10 published indices and 14 newly developed three-band SRIs, were examined (Table 2). The 3D contour maps showed statistical metrics as determination coefficients (R^2) between physical parameters such as L*, a*, b*, and Chlm as well as chemical parameters such as TSS and TSS/acid of navel orange samples and three-band SRIs (Figure 2). Based on the coefficient of determination for all three wavelength combi-

nations, the 3D contour map in Figure 2 displays more reliable and strong relationships between newly developed three-band SRIs and orange fruit quality parameters. The contour plotting was performed in all possible combinations within 390–750 nm using several three-band SRIs, and their relationships with fruit quality parameters were evaluated to discover the optimum SRIs.

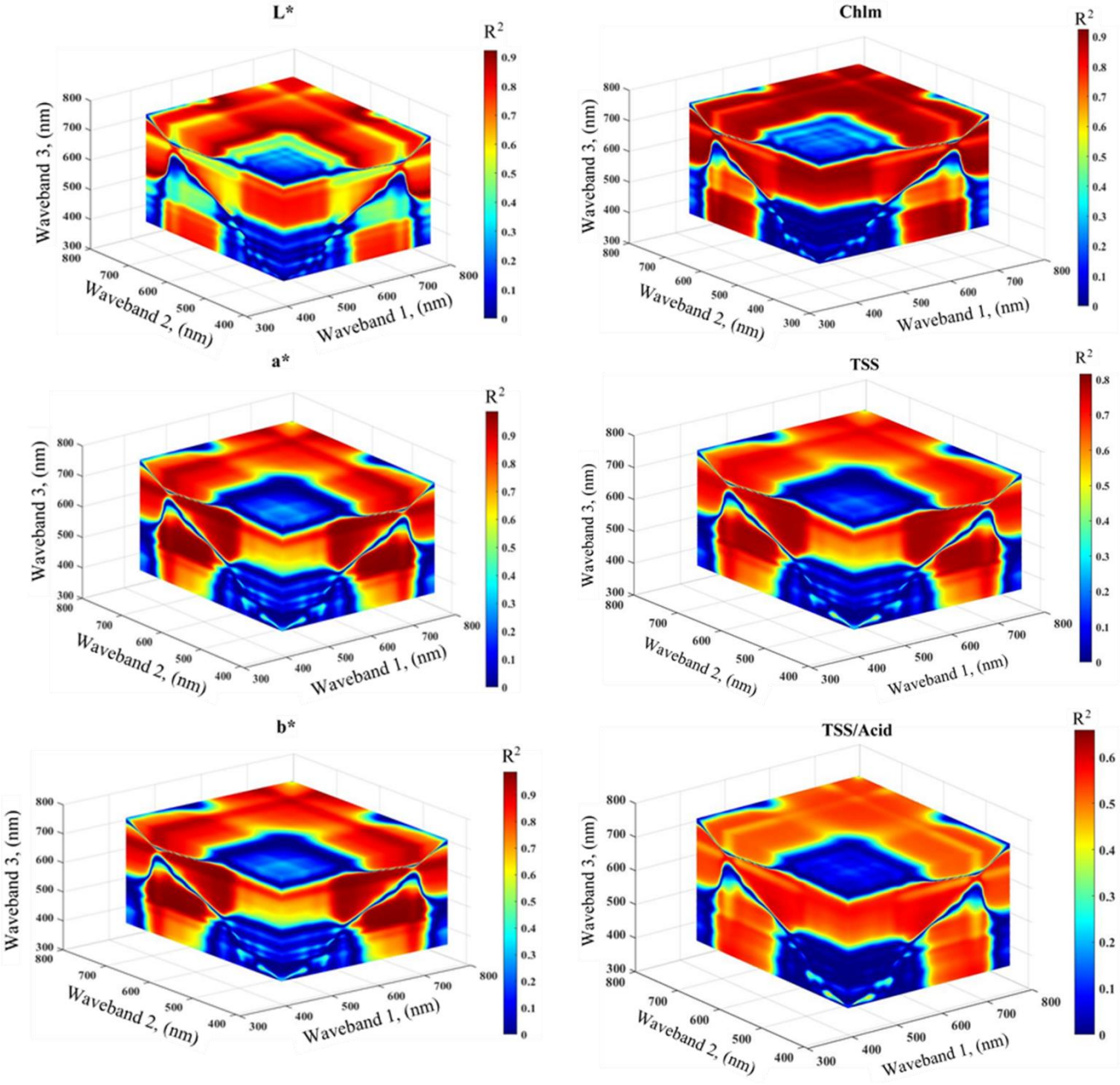


Figure 2. Three-dimensional contour maps displaying estimated coefficient of determination (R^2) values for all possible three-band combinations of the spectra with red–green (a), blue–yellow (b), brightness (L), chlorophyll meter (Chlm), total soluble solids (TSS), and TSS/acid of navel orange samples at various stages of ripening.

According to Elsayed et al. [53], 3D maps of spectral reflectance were created using the following equation:

$$\text{Normalized difference index NDI} = (R_1 - R_2 - R_3)/(R_1 + R_2 + R_2) \quad (4)$$

where R_1, R_2, and R_3 represent the values of spectral reflectance at selected wavelengths.

The existing maps are important for finding the optimal spectral area with effective wavelengths and recognizing the importance of three-band SRIs (Table 3).

Table 2. Description of different published and newly developed three-band SRIs tested in this study.

SRIs	Formula	Reference
Published SRIs		
Normalized difference index ($NDI_{570, 540}$)	$(R_{570}-R_{540})/(R_{570}+R_{540})$	[11]
Normalized difference index ($NDI_{686, 620}$)	$(R_{686}-R_{620})/(R_{686}+R_{620})$	[11]
Anthocyanin index (NAI)	$(R_{760}-R_{720})/(R_{760}+R_{720})$	[54]
$NDI_{780, 550}$	$(R_{780}-R_{550})/(R_{780}+R_{550})$	[55]
Greenness index (GI)	R_{554}/R_{677}	[56]
Pigment-sensitive ripening monitoring index (PRMI)	$(R_{750}-R_{678})/R_{550}$	[14]
Normalized chlorophyll index (NCI)	$(R_{750}-R_{678})/(R_{750}+R_{678})$	[14]
Normalized difference index ($NDI_{800, 640}$)	$(R_{800}-R_{640})/(R_{800}+R_{640})$	[12]
Normalized difference index ($NDI_{826, 670}$)	$(R_{826}-R_{670})/(R_{826}+R_{670})$	[12]
Normalized difference index ($NDI_{970, 670}$)	$(R_{970}-R_{670})/(R_{970}+R_{670})$	[12]
New three-band SRIs		
Normalized difference index ($NDI_{574,592,724}$)	$(R_{574}-R_{592}-R_{724})/(R_{574}+R_{592}+R_{724})$	This work
Normalized difference index ($NDI_{572,584,724}$)	$(R_{572}-R_{584}-R_{724})/(R_{572}+R_{584}+R_{724})$	
Normalized difference index ($NDI_{574,722,590}$)	$(R_{574}-R_{722}-R_{590})/(R_{574}+R_{722}+R_{590})$	
Normalized difference index ($NDI_{526,664,700}$)	$(R_{526}-R_{664}-R_{700})/(R_{526}+R_{664}+R_{700})$	
Normalized difference index ($NDI_{524,700,664}$)	$(R_{524}-R_{700}-R_{664})/(R_{524}+R_{700}+R_{664})$	
Normalized difference index ($NDI_{628,412,694}$)	$(R_{628}-R_{412}-R_{694})/(R_{628}+R_{412}+R_{694})$	
Normalized difference index ($NDI_{628,410,694}$)	$(R_{628}-R_{410}-R_{694})/(R_{628}+R_{410}+R_{694})$	
Normalized difference index ($NDI_{580,568,594}$)	$(R_{580}-R_{568}-R_{594})/(R_{580}+R_{568}+R_{594})$	
Normalized difference index ($NDI_{578,590,566}$)	$(R_{578}-R_{590}-R_{566})/(R_{578}+R_{590}+R_{566})$	
Normalized difference index ($NDI_{620,616,630}$)	$(R_{620}-R_{616}-R_{630})/(R_{620}+R_{616}+R_{630})$	
Normalized difference index ($NDI_{568,550,600}$)	$(R_{568}-R_{550}-R_{600})/(R_{568}+R_{550}+R_{600})$	
Normalized difference index ($NDI_{596,598,594}$)	$(R_{596}-R_{598}-R_{594})/(R_{596}+R_{598}+R_{594})$	
Normalized difference index ($NDI_{624,632,620}$)	$(R_{624}-R_{632}-R_{620})/(R_{624}+R_{632}+R_{620})$	
Normalized difference index ($NDI_{596,588,604}$)	$(R_{596}-R_{588}-R_{604})/(R_{596}+R_{588}+R_{604})$	

Table 3. Minimum (Min), maximum (Max), mean, and standard deviation (SD) of the different measured physical parameters (brightness (L*), red–green (a*), blue–yellow (b*), and chlorophyll meter (Chlm)) as well as chemical parameters (total soluble solids (TSS) and (TSS/acid)) of navel orange samples at different ripening degrees.

Degree	Statis.	L*	a*	b*	Chlm	TSS	TSS/acid
Mature	Min	49.54	−14.25	33.87	24.30	6.85	4.28
	Max	61.04	−9.15	46.75	45.60	8.60	9.51
	Mean	54.37 b	−11.24 c	39.37 c	36.42 a	7.36 c	7.16 c
	SD	3.61	1.36	4.18	6.94	0.41	1.45
Semi-ripening	Min	59.44	−6.45	49.83	4.95	6.70	6.67
	Max	70.45	6.85	63.95	17.10	11.65	16.20
	Mean	65.91 a	−0.15 b	58.53 b	10.14 b	8.94 b	11.64 b
	SD	2.53	3.91	3.75	3.61	1.14	2.61
Ripening	Min	60.92	15.27	62.83	0.00	8.70	8.57
	Max	73.35	31.06	71.89	0.00	13.95	19.89
	Mean	67.58 a	22.09 a	67.23 a	0.00 c	11.50 a	13.51 a
	SD	3.20	4.75	2.55	0.00	1.15	2.76

According to Duncan's multiple range test at a 0.05 significance level, the mean value for each parameter that has the same letter is not statistically different at various ripening degrees.

2.6. Decision Tree (DT)

The technique of learning decision trees from class-labeled training tuples is known as decision tree induction. A decision tree is a type of tree structure that resembles a flowchart. The DT algorithm's structure is made up of numerous nodes, including a root, a decision, and a leaf. The root node commences the tree, whereas the decision nodes are in charge of making decisions, i.e., moving from one node to another. The leaf nodes are yielded from the decision nodes. Some decision tree algorithms can only create binary trees (trees with exactly two internal nodes), whereas others can build nonbinary trees [57]. There were three factors taken into consideration during training, namely the maximum depth (Md) of the tree, the minimum sample leaf (Ms), and the maximum leaf nodes (Mln). The parameters values were (1, 3, 5, 7, 9), (2, 4, 6, 8, 10), and (none, 10, 20, 30, 40, 50) for Md, Ms, and Mln, respectively. The hyperparameter optimization was performed during the training, and the top-level model was generated using the best parameters. Regression rules can be simply converted from decision trees. Because the building of decision tree regressors does not need any domain expertise or parameter configuration, it is suitable for exploratory knowledge discovery.

2.6.1. Implementation of the Planned Approaches

In this research, a traditional machine learning algorithm such as DT was suggested to improve quality parameter monitoring in orange fruits. The suggested structure incorporates the following consecutive steps, as shown in Figure 3: (a) RGB image prepossessing; (b) using color RGB indices and 2D and 3D spectral indices as inputs to the DT model, divide the dataset and train based on LOOCV approach; (c) examine the performance of the model; and (d) to improve performance, adjust the hyperparameters and save the superior model. One of the focuses of this study was to examine various regression models with different RGB and spectral features in order to select the best one. We fine-tuned the model by focusing on the most important hyperparameters. These constraints were Md, Ms, and Mln to optimize the training of the DT model. Generally, the different characteristics were fed to the model randomly in the 1st iteration, the low-level parameters were dropped during each iteration, and the superb parameters were kept with respect to the highest contribution. Then, all model outcomes were compared to decide on high-quality parameters with a minimal model loss for accurate quality parameter monitoring in orange fruits.

2.6.2. Datasets and Software for Data Analysis

A total of 120 orange samples were split into training, cross-validation, and testing where 70% (84 samples) were utilized to train and validate the regression model while the other 30% (36 samples) were used to test the model's performance by comparing the predicted values with the calculated values. A leave-one-out cross-validation (LOOCV) approach was utilized to train and validate the model. LOOCV excludes one sample for validation and uses the rest of the samples for training in every trial. This method can decrease overfitting and permit a more accurate assessment of model prediction strength [58,59]. The software of Python 3.7.3 was used for image preprocessing, model building, and data analysis. The DT module from the Scikit-learn package edition 0.20.2 was investigated for regression tasks. This data analysis was carried out on a PC with a 2.4 GHz Intel Core i7-3630QM processor and 8 GB of RAM.

2.6.3. Model Evaluation

To check the performance of the regression model, the following statistical indicators were selected: coefficient of determination (R^2) and root mean square error (RMSE) [60,61]. All parameters are elucidated as follows: F_{act} is the actual value that was estimated from laboratory calculations, F_p is the predicted or simulated value, F_{ave} is the average value, and N is the total number of data points.

Root mean square error:

$$RMSE = \sqrt{\frac{1}{N}\sum_{i=1}^{N}(F_{act} - F_p)^2} \quad (5)$$

Coefficient of determination:

$$R^2 = \frac{\sum(F_{act} - F_p)^2}{\sum(F_{act} - F_{ave})^2} \quad (6)$$

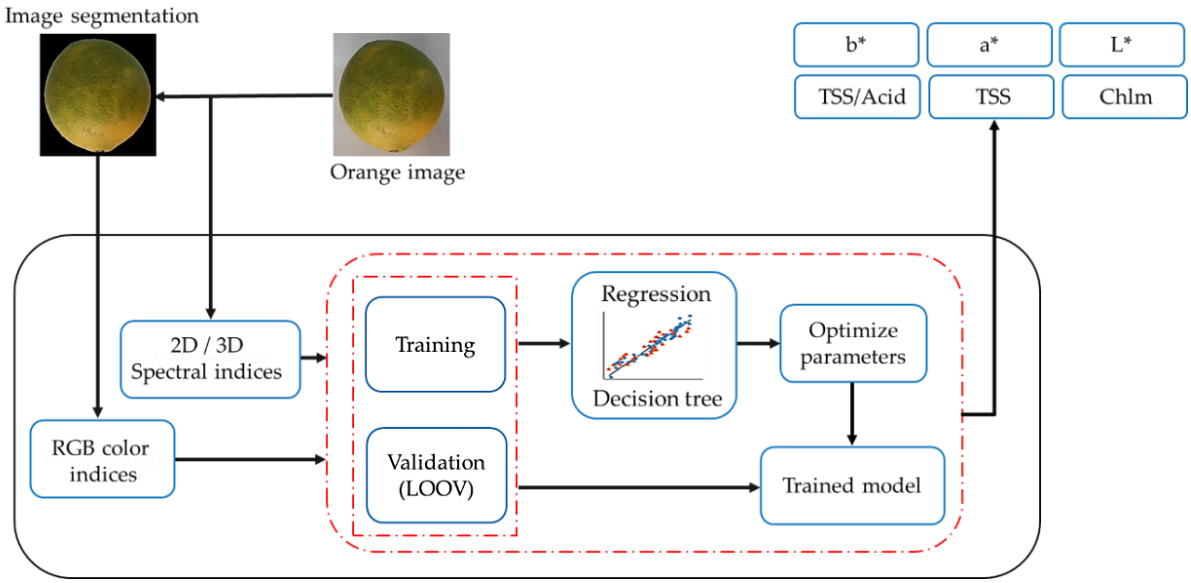


Figure 3. Flowchart for predicting the six orange fruit parameters (brightness (L*), red–green (a*), blue–yellow (b*), and chlorophyll meter (Chlm)) as well as chemical parameters (total soluble solids (TSS) and (TSS/acid)) using the DT model based on various features such as color RGB indices and 2D and 3D spectral indices.

3. Results and Discussion

3.1. Physical and Chemical Parameter Variation and Correlation Analysis for Orange Fruits

All physical parameter values such as L*, a*, b*, and expected Chlm as well as chemical parameters such as TSS and TSS/acid of navel orange samples increased during fruit ripening. There was a significant variation in the mean values of each physical and chemical parameter at different stages of ripening (Table 3). The findings demonstrated a broad range of mean values for all measured parameters at various stages of fruit ripening. The L* values ranged from 49.54 to 73.35, a* ranged from −14.25 to 31.06, b* ranged from 33.87 to 71.89, Chlm ranged from 45.60 to 0, TSS ranged from 6.70 to 13.95 (%), and TSS/acid ranged from 4.28 to 19.89. The four physical parameters L*, a*, b*, and Chlm are good indicators for the peel color. Changes occur in fruit color, which is a crucial factor influencing customer acceptance as it is considered one of the primary indicators of fruit ripeness [62,63]. This variation is a result of changes in peel pigments, including green chlorophylls and yellow, orange, and red carotenoids, during the ripening process [62]. The TSS value ranged from low at the mature stage (mean value: 7.37%) to high at the ripening stage (mean value: 11.35%). The cause is that during the ripening process, starch undergoes enzymatic hydrolysis, which converts it into simple sugars [12,13,64]. In addition, the TSS/acid ratio increased due to an increase in TSS levels and a decrease in TA values throughout the ripening process since organic acids frequently deteriorate with ripening due to respiration or conversion to sugars [65].

Table 4 displays the r-values for the physical and chemical parameters of orange fruits. The results of correlation analysis revealed a significant correlation between all

six measured parameters of orange fruits. The five measured parameters (L*, a*, b*, TSS, and TSS/acid) were shown to be positively correlated with one another and negatively correlated with Chlm. Strong correlations, ranging from 0.60 to 0.94, were found between all measured parameters of orange fruit. Elsayed et al. [12] and Galal et al. [13] also found strong negative correlations between Chl parameters and TSS of orange and banana fruit at different ripening stages, and these parameters might be employed as a ripening indicator in accordance with these findings.

Table 4. Correlations between six physical and chemical parameters (brightness (L*), red–green (a*), blue–yellow (b*), and chlorophyll meter (Chlm)) as well as chemical parameters (total soluble solids (TSS) and (TSS/acid)) of navel orange.

	L*	a*	b*	Chlm	TSS	TSS/Acid
L*	1					
a*	0.67 **	1				
b*	0.94 **	0.86 **	1			
Chlm	−0.88 **	−0.85 **	−0.94 **	1		
TSS	0.64 **	0.90 **	0.81 **	−0.78 **	1	
TSS/Acid	0.60 **	0.74 **	0.74 **	−0.73 **	0.83 **	1

** Correlation is significant at the 0.01 level (2-tailed).

3.2. Variation of RGB Indices and Spectral Indices of Orange Fruits at Different Ripening Degrees

RGB of digital image indices and SRIs were generally affected by fruit ripening degrees. This finding shows that the various phases of fruit ripening had a discernible impact on the color characteristics of orange fruit, demonstrating the viability of employing RGB as a practical and affordable monitoring technique for determining fruit quality criteria. These color variations are caused by observable changes in various biophysical fruit qualities during the ripening process, which finally produce significant alterations in the fruit's reactions to visible light [11,28,30]. The outcomes showed a considerable variation between the minimum and maximum values for RGB of the digital image analysis and SRIs (Tables 5 and 6). For example, G% values ranged from 0.319 to 0.481, GBRI ranged from 0.594 to 1.142, WI ranged from −0.250 to 1.264, EXGR ranged from 0.070 to 0.844, and COM ranged from 6.379 to 7.093. All RGB indices except R% showed a significant difference in the mean values at different ripping degrees. The values of RGB indices showed decreasing or increasing from mature to ripening degrees (Table 5).

Table 5. Minimum (Min), maximum (Max), mean, and standard deviation (SD) of the 10 RGB indices of navel orange at different ripening degrees.

Degree	Statis.	R%	G%	B%	GBRI	WI	EXG	EXB	EXGR	VEG	COM
Mature	Min	0.058	0.423	0.371	1.043	−0.250	0.271	0.096	0.407	1.722	6.596
	Max	0.205	0.481	0.462	1.142	−0.047	0.443	0.166	0.844	4.408	7.093
	Mean	0.141 a	0.450 a	0.408 c	1.104 a	−0.144 c	0.350 a	0.122 c	0.602 a	2.372 a	6.753 a
	SD	0.036	0.014	0.022	0.028	0.051	0.043	0.018	0.108	0.578	0.111
Semi-ripening	Min	0.087	0.383	0.410	0.787	−0.012	0.149	0.162	0.340	1.766	6.559
	Max	0.177	0.434	0.500	1.010	0.408	0.301	0.299	0.585	3.046	6.816
	Mean	0.140 a	0.403 b	0.456 b	0.889 b	0.200 b	0.210 b	0.235 b	0.418 b	2.004 b	6.618 b
	SD	0.020	0.013	0.022	0.062	0.118	0.038	0.038	0.060	0.301	0.060

Table 5. *Cont.*

Degree	Statis.	R%	G%	B%	GBRI	WI	EXG	EXB	EXGR	VEG	COM
Ripening	Min	0.126	0.319	0.505	0.594	0.742	−0.045	0.356	0.070	1.415	6.379
	Max	0.149	0.352	0.539	0.695	1.264	0.055	0.432	0.224	1.740	6.488
	Mean	0.138 a	0.341 c	0.521 a	0.654 c	0.900 a	0.021 c	0.389 a	0.168 c	1.585 c	6.446 c
	SD	0.006	0.008	0.010	0.026	0.123	0.024	0.021	0.034	0.063	0.023

According to Duncan's multiple range test at a 0.05 significance level, the mean value for each parameter that has the same letter is not statistically different at various ripening degrees.

Table 6. Variation in the values of SRIs at different ripening degrees.

Degree	Statis.	$NDI_{570, 540}$	$NDI_{686, 620}$	NAI	$NDI_{780, 550}$	GI	PRMI	NCI	$NDI_{800, 640}$	$NDI_{826, 670}$	$NDI_{970, 670}$	$NDI_{574,592,724}$	$NDI_{572,584,724}$
Mature	Min	−0.062	−0.227	0.082	0.360	3.055	1.818	0.748	0.558	0.742	0.692	−0.652	−0.646
	Max	−0.017	−0.093	0.179	0.597	4.702	3.634	0.867	0.799	0.872	0.845	−0.501	−0.499
	Mean	−0.039 c	−0.185 c	0.120 a	0.477 a	3.769 a	2.589 a	0.827 a	0.709 a	0.831 a	0.795 a	−0.577 b	−0.573 b
	SD	0.009	0.030	0.023	0.051	0.405	0.377	0.025	0.048	0.027	0.031	0.031	0.030
Semi-ripening	Min	0.014	−0.178	0.014	0.228	1.114	0.742	0.297	0.178	0.298	0.189	−0.485	−0.484
	Max	0.098	−0.046	0.069	0.357	2.557	1.653	0.669	0.479	0.672	0.599	−0.418	−0.419
	Mean	0.056 b	−0.128 b	0.036 b	0.286 b	1.803 b	1.240 c	0.527 b	0.342 b	0.526 b	0.438 b	−0.449 a	−0.450 a
	SD	0.023	0.036	0.014	0.034	0.399	0.246	0.105	0.087	0.104	0.114	0.019	0.019
Ripening	Min	0.088	−0.079	−0.011	0.182	0.389	0.035	0.011	0.024	0.017	−0.195	−0.507	−0.508
	Max	0.347	0.061	0.021	0.509	1.230	0.914	0.367	0.226	0.365	0.259	−0.389	−0.390
	Mean	0.225 a	0.031 a	0.000 c	0.329 b	0.612 c	0.173 b	0.050 c	0.058 c	0.059 c	−0.071 c	−0.440 a	−0.441 a
	SD	0.068	0.028	0.006	0.090	0.173	0.179	0.074	0.041	0.072	0.082	0.031	0.031
Degree	**Statis.**	$NDI_{574,722,590}$	$NDI_{526,664·700}$	$NDI_{524,700,664}$	$NDI_{628,412,694}$	$NDI_{628,410,694}$	$NDI_{580,568,594}$	$NDI_{578,590,566}$	$NDI_{620,616,630}$	$NDI_{568,550,600}$	$NDI_{596,598,594}$	$NDI_{624,632,620}$	$NDI_{596,588,604}$
Mature	Min	−0.642	−0.316	−0.341	−0.499	−0.337	−0.353	−0.353	−0.332	−0.305	−0.334	−0.334	−0.336
	Max	−0.496	−0.271	−0.293	−0.250	−0.203	−0.341	−0.339	−0.331	−0.290	−0.333	−0.332	−0.333
	Mean	−0.570 b	−0.289 a	−0.312 a	−0.379 c	−0.282 c	−0.348 c	−0.347 c	−0.331 a	−0.295 a	−0.333 b	−0.333 a	−0.334 c
	SD	0.029	0.013	0.013	0.047	0.025	0.002	0.003	0.000	0.003	0.000	0.000	0.001
Semi-ripening	Min	−0.481	−0.521	−0.536	−0.249	−0.204	−0.337	−0.335	−0.334	−0.332	−0.333	−0.335	−0.333
	Max	−0.417	−0.356	−0.374	−0.099	−0.092	−0.328	−0.325	−0.332	−0.307	−0.333	−0.334	−0.331
	Mean	−0.447 a	−0.436 b	−0.454 b	−0.157 b	−0.137 b	−0.332 b	−0.329 b	−0.333 b	−0.318 b	−0.333 a	−0.334 b	−0.332 b
	SD	0.018	0.049	0.049	0.037	0.028	0.002	0.003	0.001	0.007	0.000	0.000	0.000
Ripening	Min	−0.504	−0.841	−0.849	−0.107	−0.097	−0.329	−0.326	−0.338	−0.378	−0.333	−0.336	−0.332
	Max	−0.389	−0.514	−0.529	−0.077	−0.070	−0.324	−0.321	−0.333	−0.328	−0.333	−0.334	−0.329
	Mean	−0.439 a	−0.718 c	−0.730 c	−0.093 a	−0.085 a	−0.326 a	−0.323 a	−0.336 c	−0.349 c	−0.333 a	−0.335 c	−0.331 a
	SD	0.031	0.078	0.076	0.008	0.007	0.001	0.001	0.001	0.012	0.000	0.000	0.001

According to Duncan's multiple range test at a 0.05 significance level, the mean value for each parameter that has the same letter is not statistically different at various ripening degrees.

Figure 4 depicts the association between wavelength and reflectance collected from different orange fruit samples at different ripening degrees. The results demonstrated considerable significant variations in the respective spectral characteristics of orange fruit skin related to the reflectance values over visible (VIS) and near-infrared (NIR) ranges, as shown in Figure 4 and Table 6. The results also revealed a little change in the combined shape of the spectral signature and wavelength-locality between 400 and 500 nm. The difference in spectra in the green and red ranges (500–700 nm) was higher than the difference in the blue range (400–500 nm). The results show that the difference in spectral signature between fruit samples at different ripening degrees in the NIR region is the highest of all the electromagnetic spectrum. The change in the composite shape of the spectral signature recorded in the Vis and NIR from different fruit samples appears to be a result of color absorption and cell structure at varying ripening degrees. At different stages of ripening, the values of various SRIs showed dramatic and significant changes. As seen in the abovementioned Table 6, there were clear considerable variances in SRI values at different ripening degrees, which might have been due to large variations in physical and chemical values as shown in Table 4. For example, quantitative analyses revealed that the mean values of the new three-band SRIs such as $NDI_{526,664,700}$, $NDI_{628,412,694,}$ and $NDI_{580,568,594}$ in Table 6 significantly changed from −0.841 to −0.271, from −0.499 to −0.077, and from −0.353 to −0.324, respectively. SRI readings that progressively increase or decrease are associated with variations in the metrics measuring fruit quality in oranges at various stages of ripeness. Generally, the spectral characteristics of orange fruit skin at different ripening

degrees demonstrate significant changes in the SRI values. Several studies have found that changes in color and texture, as well as other physical and chemical characteristics of the fruits, are connected to the optical qualities of the fruit surface [13,14,56,66–68]. According to Abbott [69] and Solovchenko et al. [70], light scattering is connected to the quantity of pigment that accumulates in the thick layer of the parenchyma of various fruits.

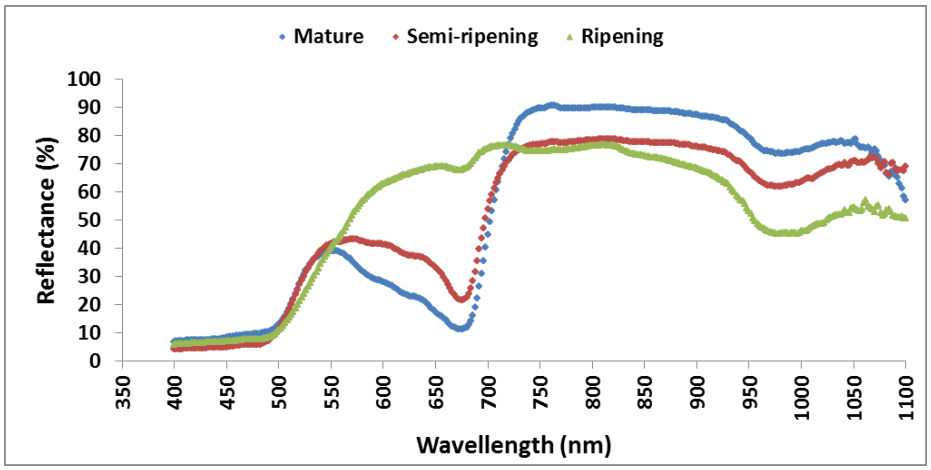


Figure 4. Spectra signature of navel orange fruit samples at different ripening degrees.

3.3. Evaluation of RGB Indices and Published and Newly Developed Three-Band SRIs to Assess the Physical and Chemical Parameters

Table 7 shows that the RGB indices (except R%) and the published and newly developed three-band SRIs had significant relationships with physical and chemical parameters at various ripening degrees. The RGB indices presented R^2 values that varied from 0.16 to 67, from 0.44 to 0.94, from 0.28 to 89, from 0.42 to 0.84, from 0.29 to 0.79, and from 0.27 to 0.54 for L*, a*, b*, Chlm, TSS, and TSS/TA, respectively. The newly developed three-band SRIs recorded R^2 values that varied from 0.44 to 90, from 0.41 to 0.97, from 0.62 to 94, from 0.59 to 0.92, from 0.38 to 0.81, and from 0.38 to 0.66 for L*, a*, b*, Chlm, TSS, and TSS/acid, respectively. According to the findings in Table 7, it is obvious that the new three-band SRIs are more successful at evaluating various fruit quality indicators. Furthermore, the RGB indices and published SRIs demonstrated satisfactory relationships in determining the selected six measured parameters. This was similar to the results of Elsayed et al. [12], who indicated that the two-band SRI ($NDVI_{780,570}$) was strongly related to total chlorophyll with an R^2 value of 0.81 and NAI was strongly related to SSC with an R^2 value of 0.81 for orange fruits. According to Galal et al. [13], the banana fruits' SRIs that were derived from VIS/VIS, VIS/NIR, and NIR/NIR wavelengths had the best R^2 with respect to biochemical parameters. The greatest R^2 values for total soluble solids (TSS) and firmness were demonstrated by $RSI_{450,640}$, which was derived from the blue and red regions of the visible spectrum. Spectral measurements of surface samples were measured by the passive reflectance sensor, and then fruit firmness was measured on two opposite sides of each fruit after a piece of peel was removed. Merzlyak et al. [71] pointed out that bands between 700 and 705 nm and spectral area between 550 and 650 nm are sensitive to changes in the chlorophyll content. Additionally, Elsayed et al. [11] found that the normalized difference vegetation index (red + blue) was associated with chlorophyll b, carotenoids, soluble solids content, and titratable acidity of mango fruits with R^2 values of 0.57, 0.53, 0.57, and 0.59, respectively. In general, the new three-band SRIs had the greatest R^2 values when compared with the values produced from the RGB indices and published SRIs. For example, $NDI_{574,592,724}$, $NDI_{572,584,724}$, and $NDI_{574,722,590}$ showed the highest R^2 value (0.90) with L*; $NDI_{526,664,700}$ and $NDI_{524,700,664}$ showed the highest R^2 value (0.97) with a*; $NDI_{628,410,694}$, $NDI_{580,568,594}$, and $NDI_{578,590,566}$ showed the highest R^2 value (0.94) with b* and (0.92) with Chlm; $NDI_{568,550,600}$ showed the highest R^2 value (0.81) with TSS;

and $NDI_{596,588,604}$ showed the highest R^2 value (0.66) with TSS/acid. From the results, it is obvious the new three-band indices based on the wavelengths from blue, green, red, red-edge, and NIR are sensitive for estimating the six measured parameters in this study. The information obtained will be crucial for supporting ongoing efforts to use specific spectral devices for carrying out precision fruit quality practices. This type of study has rarely focused on using three-band SRIs by establishing 3D contour maps to assess the fruit quality parameters at different ripening degrees.

Table 7. Relationships of linear regression of six biochemical parameters with several RGB indices and SRIs of navel orange fruits expressed as determination coefficients.

RGB Index	L*	a*	b*	Chlm	TSS	TSS/Acid
R%	0.05	0.00	0.03	0.00	0.01	0.00
G%	0.53 ***	0.92 ***	0.78 ***	0.80 ***	0.74 ***	0.54 ***
B%	0.61 ***	0.83 ***	0.83 ***	0.72 ***	0.74 ***	0.48 ***
GBRI	0.67 ***	0.91 ***	0.89 ***	0.84 ***	0.78 ***	0.55 ***
WI	0.53 ***	0.94 ***	0.79 ***	0.73 ***	0.78 ***	0.50 ***
EXG	0.53 ***	0.92 ***	0.78 ***	0.80 ***	0.74 ***	0.54 ***
EXB	0.62 ***	0.92 ***	0.86 ***	0.80 ***	0.79 ***	0.53 ***
EXGR	0.45 ***	0.85 ***	0.67 ***	0.74 ***	0.66 ***	0.50 ***
VEG	0.16 *	0.44 ***	0.28 **	0.42 ***	0.29 **	0.27 **
COM	0.37 ***	0.75 ***	0.56 ***	0.67 ***	0.56 ***	0.44 ***
$NDI_{570, 540}$	0.42 ***	0.95 ***	0.71 ***	0.70 ***	0.79 ***	0.55 ***
$NDI_{686, 620}$	0.38 ***	0.90 ***	0.63 ***	0.62 ***	0.70 ***	0.42 ***
NAI	0.81 ***	0.73 ***	0.92 ***	0.89 ***	0.63 ***	0.54 ***
$NDI_{780, 550}$	0.77 ***	0.15 *	0.55 ***	0.52 ***	0.13 *	0.17 *
GI	0.69 ***	0.83 ***	0.88 ***	0.88 ***	0.71 ***	0.59 ***
PRMI	0.76 ***	0.82 ***	0.91 ***	0.88 ***	0.70 ***	0.52 ***
NCI	0.59 ***	0.92 ***	0.81 ***	0.78 ***	0.75 ***	0.49 ***
$NDI_{800, 640}$	0.74 ***	0.86 ***	0.91 ***	0.89 ***	0.72 ***	0.54 ***
$NDI_{826, 670}$	0.60 ***	0.92 ***	0.82 ***	0.79 ***	0.75 ***	0.49 ***
$NDI_{970, 670}$	0.60 ***	0.92 ***	0.82 ***	0.80 ***	0.75 ***	0.51 ***
$NDI_{574,592,724}$	0.90 ***	0.44 ***	0.83 ***	0.80 ***	0.39 ***	0.38 ***
$NDI_{572,584,724}$	0.90 ***	0.43 ***	0.83 ***	0.79 ***	0.38 ***	0.38 ***
$NDI_{574,722,590}$	0.90 ***	0.44 ***	0.83 ***	0.80 ***	0.39 ***	0.38 ***
$NDI_{526,664,700}$	0.45 ***	0.97 ***	0.73 ***	0.71 ***	0.79 ***	0.54 ***
$NDI_{524,700,664}$	0.44 ***	0.97 ***	0.72 ***	0.71 ***	0.79 ***	0.53 ***
$NDI_{628,412,694}$	0.83 ***	0.69 ***	0.93 ***	0.91 ***	0.62 ***	0.55 ***
$NDI_{628,410,694}$	0.83 ***	0.73 ***	0.94 ***	0.92 ***	0.65 ***	0.56 ***
$NDI_{580,568,594}$	0.82 ***	0.75 ***	0.94 ***	0.92 ***	0.65 ***	0.56 ***
$NDI_{578,590,566}$	0.80 ***	0.76 ***	0.94 ***	0.92 ***	0.66 ***	0.57 ***
$NDI_{620,616,630}$	0.49 ***	0.93 ***	0.76 ***	0.73 ***	0.80 ***	0.58 ***
$NDI_{568,550,600}$	0.48 ***	0.94 ***	0.75 ***	0.75 ***	0.81 ***	0.56 ***
$NDI_{596,598,594}$	0.52 ***	0.41 ***	0.62 ***	0.59 ***	0.43 ***	0.56 ***
$NDI_{624,632,620}$	0.55 ***	0.75 ***	0.77 ***	0.74 ***	0.70 ***	0.65 ***
$NDI_{596,588,604}$	0.59 ***	0.75 ***	0.80 ***	0.76 ***	0.71 ***	0.66 ***

*, **, and ***, statistically significant at $p \leq 0.05$, $p \leq 0.01$, and $p \leq 0.00$, respectively.

3.4. Performance of Decision Tree Model Based on RGB Indices and Published and Newly Developed Three-Band SRIs for Predicting the Fruit Quality Parameters

Although RGB indices and SRIs are basic tools, and numerous indices have been successfully utilized in predicting fruit quality parameters, they are limited to a few bands and are influenced by ambient variables and timeframes [56,72–74]. Furthermore, combining various wavebands responsive to fruit quality parameters via RGB indices and SRIs with DT models should improve the models' ability to predict fruit quality parameters. Therefore, this study evaluated several DT models based on selected RGB indices or SRIs and their combinations. According to the findings, the spectral reflectance indices (SRIs) and color RGB (CIs) indices were the best integrations to filter the highest variables, as

shown in Table 8. These indices performed well in determining the quality attributes of orange fruits. As shown in Table 8, the decision tree model was trained using the CIs and 2D and 3D SRIs (independent variables) to predict the examined parameters (dependent variables). The predicted values were then compared to the reserved values for the DT model that were not implemented. This study analyzed multivariate approaches and clearly compared the findings, indicating that using multivariate methods considerably improves predictability. Because validation data are not used in the model construction process, independent validation is the most robust way for evaluating the accuracy of the regression model. The results indicated that the DT-SRIs-CIs-8 was the strongest predictive model, with a stronger link between the outstanding traits and L*. The eight various features involved in this model are of great significance for predicting L*. Its outputs with R^2 were 0.904 (RMSE = 1.470) and 0.779 (RMSE = 3.208) for cross-validation and test set, respectively. The DT-SRIs-CIs-30 model performed best in terms of measuring a*. The R^2 value was 0.98 and RMSE = 1.121 in the cross-validation, and the R^2 value was 0.964 and RMSE = 2.604 in the test set. The DT-SRIs-CIs-5 model was the most precise for recognizing b* (R^2 = 0.957 and 0.929, with RMSE = 1.713 and 3.309 for cross-validation and test set, respectively). The DT-SRIs-CIs-8 model outperformed the others in predicting Chlm. The model performance with R^2 was 0.952 (RMSE = 1.801) and 0.922 (RMSE = 4.442) for cross-validation and test set, respectively. To estimate TSS, the DT-SRIs-CIs-3 model was developed. The values of R^2 for cross-validation and test set were 0.828 (RMSE = 0.595) and 0.674 (RMSE = 1.022), respectively. The most accurate model for observing TSS/acid was the DT-CIs-SRIs-5; its R^2 outputs were 0.688 (RMSE = 1.552) and 0.484 (RMSE = 2.056) for cross-validation and test set, respectively. According to Elsherbiny et al. [75], the expected performance was improved; to update the regression methods for robust prediction, several steps were required during training, such as filtering high-level features and tuning model hyperparameters. This work sought to enhance the accuracy and resilience of the prediction model for orange fruit quality characteristics, and the integration of many features was a crucial part of that effort.

Table 8. The outputs of decision tree models (brightness (L*), red–green (a*), blue–yellow (b*), and chlorophyll meter (Chlm)) as well as chemical parameters (total soluble solids (TSS) and (TSS/acid)) of navel orange based on different indices extracted from hyperspectral and RGB images.

V	Indices	Optimal Features	Parameters (Md, Ms, Mln)	Training		Cross-Validation		Testing	
				R^2	RMSE	R^2	RMSE	R^2	RMSE
L*	Spectral	$NDI_{970, 670}$, PRMI, $NDI_{526,664,700}$, $NDI_{524,700,664}$, $NDI_{800, 640}$, $NDI_{596,598,594}$, $NDI_{686, 620}$, $NDI_{572,584,724}$, $NDI_{574,722,590}$, $NDI_{574,592,724}$	(5, 2, 10)	0.965	1.233	0.908	1.499	0.780	3.205
	RGB	ExB	(5, 4, 10)	0.898	2.106	0.805	2.238	0.880	2.371
	Total	$NDI_{524,700,664}$, VEG, PRMI, $NDI_{596,598,594}$, $NDI_{686, 620}$, $NDI_{574,592,724}$, $NDI_{572,584,724}$, ExB	(5, 2, none)	0.988	0.730	0.904	1.470	0.779	3.208

Table 8. *Cont.*

V	Indices	Optimal Features	Parameters (Md, Ms, Mln)	Training		Cross-Validation		Testing	
				R^2	RMSE	R^2	RMSE	R^2	RMSE
a*	Spectral	PRMI, $NDI_{578,590,566}$, $NDI_{826,670}$, GI, $NDI_{568,550,600}$, $NDI_{800,640}$, $NDI_{686,620}$, $NDI_{620,616,630}$, $NDI_{524,700,664}$, $NDI_{628,412,694}$, $NDI_{780,550}$, NAI, $NDI_{628,410,694}$	(5, 6, 10)	0.987	1.641	0.972	1.553	0.940	3.362
	RGB	bn, VEG, COM, ExB, ExG, GBRI, WI, ExGR	(3, 2, none)	0.984	1.852	0.956	1.903	0.959	2.774
	Total	$NDI_{526,664,700}$, $NDI_{826,670}$, rn, ExB, PRMI, $NDI_{628,410,694}$, $NDI_{596,598,594}$, VEG, $NDI_{686,620}$, NCI, $NDI_{568,550,600}$, $NDI_{800,640}$, $NDI_{572,584,724}$, $NDI_{970,670}$, $NDI_{578,590,566}$, ExG, COM, bn, $NDI_{580,568,594}$, gn, GI, ExGR, WI, $NDI_{624,632,620}$, $NDI_{524,700,664}$, $NDI_{574,592,724}$, $NDI_{628,412,694}$, $NDI_{780,550}$, NAI, GBRI	(7, 2, 40)	0.999	0.514	0.986	1.121	0.964	2.604
b*	Spectral	rn, $NDI_{574,592,724}$, GI, $NDI_{970,670}$	(5, 2, 30)	0.993	0.998	0.951	1.973	0.929	3.296
	RGB	'ExGR, GBRI	(3, 4, none)	0.968	2.162	0.949	2.057	0.951	2.739
	Total	VEG, $NDI_{628,410,694}$, $NDI_{574,722,590}$, ExGR, $NDI_{970,670}$	(7, 2, 40)	0.998	0.551	0.957	1.713	0.929	3.309
Chlm	Spectral	$NDI_{624,632,620}$, $NDI_{596,588,604}$, $NDI_{568,550,600}$, $NDI_{578,590,566}$, $NDI_{524,700,664}$, $NDI_{628,412,694}$	(7, 2, 20)	0.996	0.974	0.949	2.038	0.944	3.762
	RGB	COM, GBRI, ExG, ExGR, gn, ExB, WI	(3, 2, 10)	0.962	3.153	0.938	2.477	0.874	5.659
	Total	$NDI_{628,412,694}$, rn, $NDI_{624,632,620}$, $NDI_{568,550,600}$, $NDI_{596,588,604}$, $NDI_{578,590,566}$, $NDI_{524,700,664}$, WI	(9, 2, none)	0.998	0.722	0.952	1.801	0.922	4.442
TSS	Spectral	$NDI_{628,410,694}$, $NDI_{578,590,566}$	(5, 2, 20)	0.941	0.494	0.829	0.602	0.432	1.348
	RGB	COM, GBRI, ExG, bn, WI	(5, 4, 10)	0.911	0.606	0.792	0.661	0.705	0.971
	Total	bn, $NDI_{628,410,694}$,WI	(3, 6, none)	0.898	0.648	0.828	0.595	0.674	1.022

Table 8. *Cont.*

V	Indices	Optimal Features	Parameters (Md, Ms, Mln)	Training		Cross-Validation		Testing	
				R^2	RMSE	R^2	RMSE	R^2	RMSE
TSS/Acid	Spectral	$NDI_{580,568,594}$, $NDI_{568,550,600}$, $NDI_{596,598,594}$, $NDI_{596,588,604}$, $NDI_{628,410,694}$	(5, 2, none)	0.959	0.777	0.657	1.632	0.328	2.346
	RGB	VEG, GBRI, ExGR, bn, ExG	(7, 2, 10)	0.846	1.503	0.578	1.800	0.173	2.603
	Total	$NDI_{568,550,600}$, $NDI_{970,670}$, $NDI_{596,598,594}$, $NDI_{596,588,604}$, $NDI_{628,410,694}$	(5, 2, 10)	0.905	1.177	0.688	1.552	0.484	2.056

V is the studied variable, Md is maximum depth, Ms is minimum sample leaf, and Mln is maximum leaf nodes.

4. Conclusions

A low-cost approach for evaluating the characteristics of navel orange fruits at various stages of ripeness was developed using color RGB indices and both published and newly developed three-band SRIs combined with the DT model. These properties included some physical parameters such as L*, a*, b*, and expected Chlm as well as chemical parameters such as TSS and TSS/acid of the navel orange samples. All variable values increased during fruit ripening. The mean values of all physical and chemical parameters differed significantly during the maturation phases. In general, the newly developed three-band SRIs outperformed both the RGB indices and previously published SRIs in terms of R^2 values. Furthermore, the RGB indices and published SRIs revealed satisfactory relationships in identifying the six observed parameters. Regarding Chlm prediction, the DT-SRIs-CIs-8 model was superior to all other models. Its performance values with R^2 were 0.952 (RMSE = 1.801) and 0.922 (RMSE = 4.442) for the cross-validation and test set, respectively. Otherwise, to estimate TSS, the DT-SRIs-CIs-3 model performed well and had the highest R^2 values for the cross-validation (0.828) and test set (0.674) with the lowest RMSE values (0.595 and 1.022, respectively). Finally, combining passive sensing data with an RGB camera might aid in the creation of efficient high-throughput systems that allow low-cost data collection from a range of fruits at different stages of maturity. This knowledge, based on the best RGB indices, spectral indices, and DT calibration models obtained in this work, might be utilized to construct active sensor systems for monitoring fruit ripeness in the field or factory.

Supplementary Materials: The following supporting information can be downloaded at: https://www.mdpi.com/article/10.3390/agriculture12101558/s1, the Python code as Supplementary Materials to this paper.

Author Contributions: Conceptualization, S.E.; Methodology, S.E., H.G., M.F., O.E. and A.A.; Software, S.E., H.G., M.F. and O.E. Formal Analysis, S.E., M.F., O.E. and H.G.; Resources, S.E., Data Curation, S.E., H.G., M.F. and A.A.; Writing—Original Draft Preparation, S.E., H.G. and O.E. Writing—Review and Editing, S.E., H.G., M.F. and A.A.; Supervision, S.E.; Project Administration, S.E.; Funding Acquisition, S.E., H.G., M.F. and A.A. All authors have read and agreed to the published version of the manuscript.

Funding: The authors extend their appreciation to the University of Sadat City in Egypt for funding this research work through Project 19.

Data Availability Statement: Data of statistical analysis are presented in the article.

Acknowledgments: We would like to thank the University of Sadat City in Egypt for supporting this study within the framework of Project 19.

Conflicts of Interest: The authors declare no conflict of interest.

References

1. FAO. Food and Agricultural Organization of the United Nations. 2022. Available online: http://faostat.fao.org (accessed on 5 August 2022).
2. Egyptian Ministry of Agriculture and Land Reclamation. *Bulletin of the Agricultural Statistics Part (2)*; Summer & Nile Crops: Cairo, Egypt, 2019.
3. Huang, Y.; Lu, R.; Chen, K. Assessment of tomato soluble solids content and pH by spatially-resolved and conventional Vis/NIR spectroscopy. *J. Food Eng.* **2018**, *236*, 19–28. [CrossRef]
4. Ahmed, Z.F.R.; Taha, E.M.A.; Abdelkareem, N.A.A.; Mohamed, W.M. Postharvest properties of unripe bananas and the potential of producing economic nutritious. *Int. J. Fruit Sci. Prod.* **2020**, *20*, 995–1014. [CrossRef]
5. Bureau, S.; Scibisz, I.; le Bourvellec, C.; Renard, C.M. Effect of sample preparation on the measurement of sugars, organic acids, and polyphenols in apple fruit by mid-infrared spectroscopy. *J. Agric. Food. Chem.* **2012**, *60*, 3551–3563. [CrossRef]
6. Tadeo, J.L.; Ortiz, J.M.; Estelles, A. Sugar changes in Clementine and orange fruit during ripening. *J. Hortic. Sci.* **1987**, *62*, 531–537. [CrossRef]
7. Iglesias, D.J.; Cercós, M.; Colmenero-Flores, J.M.; Naranjo, M.A.; Ríos, G.; Carrera, E.; Ruiz-Rivero, O.; Lliso, I.; Morillon, R.; Tadeo, F.R.; et al. Physiology of citrus fruiting. *Braz. J. Plant Physiol.* **2007**, *19*, 333–362. [CrossRef]
8. Mbogo, G.; Mubofu, E.; Othman, C. Post harvest changes in physico-chemical properties and levels of some inorganic elements in off vine ripened orange (*Citrus sinensis*) fruits cv (Navel and Valencia). *Afr. J. Biotechnol.* **2010**, *9*, 1809–1815. [CrossRef]
9. Chan, L.M.; Tan, R.; Thio, G. Design of visual- based colour classification system. Research papers. *JASA* **2007**, *2*, 30–33.
10. Wang, H.; Peng, J.; Xie, C.; Bao, Y.; He, Y. Fruit quality evaluation using spectroscopy technology: A Review. *Sensors* **2015**, *15*, 11889–11927. [CrossRef]
11. Elsayed, S.; Galal, H.; Allam, A.P.; Schmidhalter, U. Passive reflectance sensing anddigital image analysis for assessing quality parameters of mango fruits. *Sci. Hortic.* **2016**, *212*, 136–147. [CrossRef]
12. Elsayed, S.; El-Gozayer, K.; Allam, A.; Schmidhalter, U. Passive reflectance sensing using regression and multivariate analysis to estimate biochemical parameters of different fruits kinds. *Sci. Hortic.* **2019**, *243*, 21–33. [CrossRef]
13. Galal, H.; Elsayed, S.; Allam, A.; Farouk, M. Indirect quantitative analysis of biochemical parameters in banana using spectral reflectance indices combined with machine learning modeling. *Horticulturae* **2022**, *8*, 438. [CrossRef]
14. Nagy, A.; Riczu, P.; Tamás, J. Spectral evaluation of apple fruit ripening and pigment content alteration. *Sci. Hortic.* **2016**, *201*, 256–264. [CrossRef]
15. Sirisomboon, P. NIR Spectroscopy for Quality Evaluation of Fruits and Vegetable. Mater. *Today Proc.* **2018**, *5*, 22481–22486.
16. He, J.G.; Luo, Y.; Liu, G.S.; Xu, S.; Si, Z.H.; He, X.G.; Wang, S.L. Prediction of soluble solids content of jujube fruit using hyperspectral reflectance imaging. In *Mechatronics and Intelligent Materials III, Pts 1–3*; Chen, R., Sung, W.P., Kao, J.C.M., Eds.; Trans. Tech. Publications: XiShuangBanNa, China, 2013; Volume 706–708, pp. 201–204.
17. Mc Clure, W.F. Near-infrared spectroscopy–the giant is running strong. *Anal. Chem.* **1994**, *66*, 43–53. [CrossRef]
18. Hashim, N.; Onwude, D.I.; Osman, M.S. Evaluation of chilling injury in mangoes using multispectral imaging. *J. Food Sci.* **2018**, *83*, 1271–1279. [CrossRef]
19. Lu, R.; Guyer, D.E.; Beaudry, R.M. Determination of firmness and sugar content of apples using near-infrared diffuse reflectance. *J. Texture Stud.* **2000**, *31*, 615–630. [CrossRef]
20. Luz, R. Near-infrared multispectral scattering. *J. Texture Stud.* **2004**, *35*, 263–276.
21. Qing, Z.; Ji, B.; Zude, M. Wavelength selection for predicting physicochemical properties of apple fruit based on near-infrared spectroscopy. *J. Food Qual.* **2007**, *30*, 511–526. [CrossRef]
22. Włodarska, K.; Szulc, J.; Khmelinskii, I.; Sikorska, E. Non-destructive determination of strawberry fruit and juice quality parameters using ultraviolet, visible, and near-infrared spectroscopy. *J. Sci. Food Agric.* **2019**, *99*, 5953–5961. [CrossRef]
23. Elsayed, S.; El-Hendawy, S.; Khadr, M.; Elsherbiny, O.; Al-Suhaibani, N.; Alotaibi, M.; Tahir, M.U.; Darwish, W. Combining thermal and RGB imaging indices with multivariate and data-driven modeling to estimate the growth, water status, and yield of potato under different drip irrigation regimes. *Remote Sens.* **2021**, *13*, 1679. [CrossRef]
24. Elsherbiny, O.; Zhou, L.; Feng, L.; Qiu, Z. Integration of Visible and Thermal Imagery with an Artificial Neural Network Approach for Robust Forecasting of Canopy Water Content in Rice. *Remote Sens.* **2021**, *13*, 1785. [CrossRef]
25. del Valle, J.C.; Gallardo-López, A.; Buide, M.L.; Whittall, J.B.; Narbona, E. Digital photography provides a fast, reliable, and noninvasive method to estimate anthocyanin pigment concentration in reproductive and vegetative plant tissues. *Ecol. Evol.* **2018**, *8*, 3064–3076. [CrossRef]
26. Ismail, W.I.W.; Razali, M.H. Machine vision to determine agricultural crop maturity. In *Trends in Vital Food and Control Engineering*; IntechOpen: London, UK, 2012; pp. 115–124.
27. Liu, Y.; Ouyang, A.; Luo, J.; Chen, X. Near infrared diffuse reflectance spectroscopy for rapid analysis of soluble solids content in navel orange. *Spectrosc. Spect. Anal.* **2007**, *27*, 2190–2192.
28. Fouda, T.; Derbala, A.; Elmetwalli, A.; Salah, S. Detection of orange color using Imaging analysis. *AgroLife Sci. J.* **2013**, *2*, 181–184.
29. Domingo, L.D.; Serrano, P.B.; Serrano, P.E.; del Rosario, E.J. Digital photometric method for Determining degree of Harvest maturity and ripeness of Sinta Papava (*Carica papaya* L.) fruits. *Philipp. Agric. Sci.* **2012**, *3*, 252–259.

30. Choi, D.; Lee, W.S.; Schueller, J.K.; Ehsani, R.; Roka, F.; Diamond, J. A Performance Comparison of RGB, NIR, and Depth Images in Immature Citrus Detection Using Deep Learning Algorithms for Yield Prediction. In *2017 ASABE Annual International Meeting*; American Society of Agricultural and Biological Engineers: St. Joseph Charter Township, MI, USA, 2017; Volume 1.
31. Gomes-Junior, F.G.; Arruda, N.; Marcos-Filho, J. Swingle citrumelo seed vigor and storability associated with fruit maturity classes. *Sci. Agric.* **2017**, *74*, 357–363. [CrossRef]
32. Beltrán, N.H.; Duarte-Mermoud, M.A.; Salah, S.A.; Bustos, M.A.; Peña-Neira, A.I.; Loyola, E.A.; Jalocha, J.W. Feature selection algorithms using Chilean wine chromatograms as examples. *J. Food Eng.* **2005**, *67*, 483–490. [CrossRef]
33. Guyon, I.; Elisseeff, A. An Introduction to Variable and Feature Selection. *J. Mach. Learn. Res.* **2003**, *3*, 1157–1182.
34. Schuize, F.H.; Wolf, H.; Jansen, H.; Vander, V.P. Applications of artificial neural networks in integrated water management: Fiction or future? *Water Sci. Technol.* **2005**, *52*, 21–31. [CrossRef]
35. ElMasry, G.; Sun, D.W.; Allen, P. Near-infrared hyperspectral imaging for predicting colour, pH and tenderness of fresh beef. *J. Food Eng.* **2012**, *110*, 127–140. [CrossRef]
36. Strobl, C.; Boulesteix, A.-L.; Kneib, T.; Augustin, T.; Zeileis, A. Conditional variable importance for random forests. *BMC Bioinform.* **2008**, *9*, 307. [CrossRef] [PubMed]
37. Glorfeld, L.W. A methodology for simplification and interpretation of backpropagation-based neural network models. *Expert Syst. Appl.* **1996**, *10*, 37–54. [CrossRef]
38. Melis, G.; Dyer, C.; Blunsom, P. On the state of the art of evaluation in neural language models. *arXiv* **2017**, arXiv:1707.05589.
39. Bergstra, J.; Yamins, D.; Cox, D. Making a science of model search: Hyperparameter optimization in hundreds of dimensions for vision architectures. In Proceedings of the 30th International Conference on Machine Learning, PMLR, Atlanta, GA, USA, 16–21 June 2013; pp. 115–123.
40. Wu, J.; Chen, X.-Y.; Zhang, H.; Xiong, L.-D.; Lei, H.; Deng, S.-H. Hyperparameter optimization for machine learning models based on Bayesian optimization. *J. Electron. Sci. Technol.* **2019**, *17*, 26–40.
41. Mc Guire, R.G. Reporting of objective color measurements. *Hortscience* **1992**, *27*, 1254–1255. [CrossRef]
42. AOAC. *Official Methods of Analysis*, 13th ed.; Association of Official Analytical Chemists: Washington, DC, USA, 1980.
43. Fauzi, M.H.; Tjandrasa, H. Implementasi thresholding citra menggunakan algoritma hybrid optimal estimation. In *Teknologi Informasi*; Institut Teknologi Sepuluh Nopember: Surabaya, Indonesia, 2010.
44. Yossya, E.H.; Pranata, J.; Wijaya, T.; Hermawan, H.; Budiharto, W. Mango Fruit Sortation System using Neural Network and Computer Vision. *Procedia Comput. Sci.* **2017**, *116*, 569–603. [CrossRef]
45. Kumaseh, M.R.; Luther, L.; Nainggolan, N. Segmentasi Citra Digital Ikan Menggunakan Metode Thresholding. *J. Ilm. Sains* **2013**, *13*, 74–79. [CrossRef]
46. Verrelst, J.; Schaepman, M.E.; Koetz, B.; Kneubuhler, M. Angular sensitivity analysis of vegetation indices derived from 726 CHRIS/PROBA data. *Remote Sens. Environ.* **2008**, *112*, 2341–2353. [CrossRef]
47. Tucker, C.J. Red and photographic infrared linear combinations for monitoring vegetation. *Remote Sens. Environ.* **1979**, *8*, 127–150. [CrossRef]
48. Woebbecke, D.; Meyer, G.; von Bargen, K.; Mortensen, D. Plant species identification, size, and enumeration using machine vision techniques on near-binary images. *Int. Soc. Opt. Photonics* **1993**, *1836*, 208–219.
49. Mao, W.; Wang, Y.; Wang, Y. Real-time detection of between-row weeds using machine vision. In Proceedings of the ASAE Annual Meeting, Las Vegas, NV, USA, 27–30 July 2003; American Society of Agricultural and Biological Engineers: St. Joseph, MI, USA, 2003; p. 1.
50. Hague, T.; Tillett, N.; Wheeler, H. Automated crop and weed monitoring in widely spaced cereals. *Precis. Agric.* **2006**, *7*, 21–32. [CrossRef]
51. Saberioon, M.M.; Amin, M.S.M.; Anuar, A.R.; Gholizadeh, A.; Wayayok, A.; Khairunniza- Bejo, S. Assessment of rice leaf chlorophyll content using visible bands at different growth stages at both the leaf and canopy scale. *Int. J. Appl. Earth Obs. Geoinf.* **2014**, *32*, 35–45. [CrossRef]
52. Guijarro, M.; Pajares, G.; Riomoros, I.; Herrera, P.J.; Burgos-Artizzu, X.P.; Ribeiro, A. Automatic segmentation of relevant textures in agricultural images. *Comput. Electron. Agric.* **2011**, *75*, 75–83. [CrossRef]
53. Elsayed, S.; Ibrahim, H.; Hussein, H.; Elsherbiny, O.; Elmetwalli, A.H.; Moghanm, F.S.; Ghoneim, A.M.; Danish, S.; Datta, R.; Gad, M. Assessment of water quality in Lake Qaroun using ground-based remote sensing data and artificial neural networks. *Water* **2021**, *13*, 3094. [CrossRef]
54. Rouse, J.W.; Haas, R.H.; Schell, J.A.; Deering, D.W.; Harlan, J.C. *Monitoring the Vernal Advancement of Retro Gradation of Natural Vegetation*; Final Report; NASA/GSFC, Type lll: Greenbelt, MD, USA, 1974.
55. Gutierrez, M.; Reynolds, M.P.; Raun, W.R.; Stone, M.L.; Klatt, A.R. Spectral water indices for assessing yield in elite bread wheat genotypes in well irrigated, water stressed, and high temperature conditions. *Crop Sci.* **2010**, *50*, 197–214. [CrossRef]
56. Acharya, U.K.; Subedi, P.P.; Walsh, K.B.; McGlasson, W.B. Estimation of fruit maturation and ripening using spectral indices. *Acta Hortic.* **2016**, *1119*, 265–272. [CrossRef]
57. Han, J.; Kamber, M. *Data Mining: Concepts and Techniques*; Morgan Kaufmann: San Francisco, CA, USA, 2001.
58. Wang, C.; Nie, S.; Xi, X.H.; Luo, S.Z.; Sun, X.F. Estimating the biomass of maize with hyperspectral and LiDAR data. *Remote Sens.* **2017**, *9*, 11. [CrossRef]

59. Zhu, J.; Huang, Z.H.; Sun, H.; Wang, G.X. Mapping forest ecosystem biomass density for Xiangjiang river basin by combining plot and remote sensing data and comparing spatial extrapolation methods. *Remote Sens.* **2017**, *9*, 241. [CrossRef]
60. Malone, B.P.; Styc, Q.; Minasny, B.; McBratney, A.B. Digital soil mapping of soil carbon at the farm scale: A spatial downscaling approach in consideration of measured and uncertain data. *Geoderma* **2017**, *290*, 91–99. [CrossRef]
61. Saggi, M.K.; Jain, S. Reference evapotranspiration estimation and modeling of the Punjab Northern India using deep learning. *Comput. Electron. Agric.* **2019**, *156*, 387–398. [CrossRef]
62. Choo, W.S. *Fruit Pigment Changes during Ripening, Encyclopedia of Food Chemistry*; Elsevier: Amsterdam, The Netherlands, 2018.
63. Khodabakhshian, R.; Khojastehpour, M. Characteristics changes of date fruits during ripening period on-palm. *Agric. Eng. Int. CIGR J.* **2021**, *23*, 243–255.
64. Maduwanthi, S.D.T.; Marapana, R.A.U.J. Induced ripening agents and their effect on fruit quality of banana. *Int. J. Food Sci.* **2019**, *2019*, 2520179. [CrossRef]
65. Rooban, R.; Shanmugam, M.; Venkatesan, T.; Tamilmani, C. Physiochemical changes during different stages of fruit ripening of climacteric fruit of mango (*Mangifera indica* L.) and non-climacteric of fruit cashew apple (*Anacardium occidentale* L.). *J. Appl. Adv. Res.* **2016**, *1*, 53–58. [CrossRef]
66. Lammertyn, J.; Peirs, A.; De Baerdemaeker, J.; Nicolai, B. Light penetration properties of NIR radiation in fruit with respect to non-destructive quality assessment. *Postharvest Biol. Technol.* **2000**, *18*, 121–132. [CrossRef]
67. Rutkowski, K.P.; Michalczuk, B.; Konopacki, P. Nondestructive determination of 'golden delicious' apple quality and harvest maturity. *J. Fruit Ornam. Plant Res.* **2008**, *16*, 39–52.
68. Abbaspour-Gilandeh, Y.; Sabzi, S.; Hernández-Hernández, M.; Hernández-Hernández, J.L.; Azadshahraki, F. Nondestructive estimation of the chlorophyll b of apple fruit by color and spectral features using different methods of hybrid artificial neural network. *Agronomy* **2019**, *9*, 735. [CrossRef]
69. Abbott, J.A. Quality measurement of fruits and vegetables. *Postharvest Biol. Technol.* **1999**, *15*, 207–225. [CrossRef]
70. Solovchenko, A.E.; Chivkunova, O.B.; Merzlyak, M.N.; Gudkovsky, V.A. Relationship between chlorophyll and carotenoid pigments during on-and off- tree ripening of apple fruits as revealed non-destructively with reflectance spectroscopy. *Postharvest Biol. Technol.* **2005**, *38*, 9–17. [CrossRef]
71. Merzlyak, M.N.; Solovchenko, A.E.; Gitelson, A.A. Reflectance spectral features and non-destructive estimation of chlorophyll, carotenoid and anthocyanin content in apple fruit. *Postharvest Biol. Technol.* **2003**, *27*, 197–211. [CrossRef]
72. Qin, J.W.; Thomas, F.B.; Zhao, X.H.; Nikhil, N.; Mark, A.R. Development of a two-band spectral imaging system for real-time citrus canker detection. *J. Food Eng.* **2012**, *108*, 87–93. [CrossRef]
73. Pourdarbani, R.; Sabzi, S.; Hernández-Hernández, M.; Hernández-Hernández, J.L.; Gallardo-Bernal, I.; Herrera-Miranda, I. Non-destructive estimation of total chlorophyll content of apple fruit based on color feature, spectral data and the most effective wavelengths using hybrid artificial neural network-imperialist competitive algorithm. *Plants* **2020**, *9*, 1547. [CrossRef] [PubMed]
74. Ringer, T.; Blanke, M. Non-invasive, real time in-situ techniques to determine the ripening stage of banana. *J. Food Meas. Charact.* **2021**, *15*, 4426–4437. [CrossRef]
75. Elsherbiny, O.; Fan, Y.; Zhou, L.; Qiu, Z. Fusion of feature selection methods and regression algorithms for predicting the canopy water content of rice based on hyperspectral data. *Agriculture* **2021**, *11*, 51. [CrossRef]